Organization of supramolecular assembly of 9-mesityl-10-carboxymethylacridinium ion and fullerene clusters on TiO$_2$ nanoparticles for light energy conversion†

Taku Hasobe,[abc] Shigeki Hattori,[ab] Prashant V. Kamat,[c] Yuji Wada[a] and Shunichi Fukuzumi*[ab]

TiO$_2$ nanoparticles modified with composite nanoclusters of 9-mesityl-10-carboxymethylacridinium ion (**Mes–Acr$^+$–COOH**) and fullerene (C$_{60}$) in acetonitrile–toluene (3 : 1, v/v) were deposited as thin films on nanostructured SnO$_2$ electrode using an electrophoretic technique. The composite TiO$_2$ films have broad as well as high absorbance properties, exhibiting a photoactive response under visible light excitation using I$_3^-$/I$^-$ redox couple, in contrast with the reference multilayer films composed of the single component. This indicates that the composite cluster TiO$_2$ film based on 9-mesityl-10-carboxymethylacridinium ion and fullerene harvests light widely in the visible region due to organization of the supramolecular assembly. In the case of a monolayer system of TiO$_2$ nanocrystallites modified with **Mes–Acr$^+$–COOH**, however, no net photocurrent is observed in the photocurrent action spectrum. This indicates that TiO$_2$ nanoparticles act as materials to organize composite molecules rather than as those to accept electrons. An incident photon-to-photocurrent generation efficiency (IPCE) of 37% has been achieved at an applied bias potential of 0.2 V *vs.* SCE in the **Mes–Acr$^+$–COOH**/C$_{60}$ composite system using TiO$_2$ nanoparticles.

Introduction

Self-assembly is the autonomous organization of components into patterns or structures, and its processes are common throughout nature and technology.[1] Molecular assembly involves a variety of interactions, presenting unique characteristics which have hardly appeared in a single molecule.[1–3] Hydrogen bonding, van der Waals interaction, and hydrophobic effects are the major driving force to achieve such ordered molecular assemblies.[4,5] Of particular interest is the ability of such assemblies in a protein matrix to mimic the energy and electron-transfer processes in the photosynthetic reaction center.[6,7]

In the past two decades, extensive endeavors have been devoted to develop molecular donor–acceptor systems (triads, tetrad, pentads, *etc.*), which can mimic a cascade of electron-transfer steps in the natural photosynthetic reaction center, leading to long-range charge separation with prolonged lifetime of the charge-separated state into second-order range.[8–12] However, synthetic difficulties have precluded application of such artificial photosynthetic model compounds to the development of low-cost photovoltaic devices.[13–15] In addition, a significant amount of energy is lost during the multi-step electron-transfer processes in both natural and artificial long-range charge separation. Avoidance of such wasted energy and high-cost multi-step synthesis is certainly required for development of low-cost efficient molecular devices. In this context, we have recently designed and synthesized a simple dyad (9-mesityl-10-methylacridinium ion) which exhibits extremely slow charge-recombination of the electron-transfer state with a remarkably high energy (2.37 eV).[16] Such a simple molecular dyad capable of fast charge separation, but extremely slow charge recombination, has obvious advantages with regard to synthetic feasibility.

On the other hand, the requirement to develop inexpensive renewable energy sources has stimulated new approaches for production of efficient, low-cost organic photovoltaic devices.[17–22] In recent years particular attention has been drawn towards the development of bulk heterojunction organic solar cells, which possess an active layer of a conjugated donor polymer and an acceptor fullerene.[21,22] Fullerene is suitable as an electron acceptor component in such organic solar cells, since electron-transfer reduction of C$_{60}$ is highly efficient because of the minimal changes of structure and solvation associated with the electron-transfer reduction.[11,12] In addition, we have recently reported light energy conversion systems based on composite molecular clusters of electron donor moieties and acceptor fullerenes by electrophoretic deposition methods.[23] These reports clearly demonstrate that three dimensional control between donor and acceptor moieties in multilayer films has a great effect on light energy conversion properties. The electrophoretic deposition methods of dye-adsorbed TiO$_2$ nanoparticles on electrodes has also been reported to be useful for the preparation of organic thin films to obtain good electron acceptor materials.[24]

However, the utilization of TiO_2 nanoparticles for three dimensional control in organization of donor–acceptor composite molecules has yet to be reported.

We report herein a new type of organic solar cell based on TiO_2 nanoparticles modified with supramolecular self-assembly clusters of 9-mesityl-10-carboxymethylacridinium ion (Fig. 1) and fullerene, which are deposited as thin films on an optically transparent electrode (OTE) of nanostructured SnO_2 (OTE/SnO_2) using an electrophoretic method. 9-Mesityl-10-methylacridinium ion (**Mes–Acr$^+$**), which exhibits slow charge-recombination of the electron-transfer state with remarkably high energy,[16] is modified with a carboxylic acid group (**Mes–Acr$^+$–COOH** in Fig. 1) and assembled on TiO_2 nanoparticles (denoted as **Mes–Acr$^+$–COO–TiO$_2$** in Fig. 1). The photoelectrochemical performance of nanostructured SnO_2 films of TiO_2 nanoparticles modified with composite clusters of **Mes–Acr$^+$–COOH** and fullerene [denoted as OTE/SnO_2/(**Mes–Acr$^+$–COO–TiO$_2$** + C_{60})$_n$] is significantly superior to the single component films of an individual component. The morphology and the photocurrent generation mechanism of OTE/SnO_2/(**Mes–Acr$^+$–COO–TiO$_2$** + C_{60})$_n$ are reported in full detail in this paper.

Experimental

General

The chemicals used in this study were of the best grade available, supplied by Tokyo Chemical Industries, Wako Pure Chemical, or Sigma Aldrich Co. ^1H NMR spectra were recorded on a JNM-AL300 (JEOL) instrument at 300 MHz. Matrix-assisted laser desorption/ionization (MALDI) time-of-flight (TOF) mass spectra were measured on a Kratos Compact MALDI I (Shimadzu). TiO_2 nanoparticles (P25, d = 21 nm) were purchased from Nippon Aerogel Co. Preparation of 9-mesityl-10-carboxymethylacridinium ion (**Mes–Acr$^+$–COOH**) has been described elsewhere,[23d] and the synthetic procedure for the reference compound (**Acr$^+$–COOH** in Fig. 1) is described in the electronic supplementary information (ESI).†

Preparation of TiO$_2$ nanoparticles modified with the dye moieties (Mes–Acr$^+$–COO–TiO$_2$ and Acr$^+$–COO–TiO$_2$)

Mes–Acr$^+$–COO–TiO$_2$ and **Acr$^+$–COO–TiO$_2$** were prepared by immersing warmed TiO_2 nanoparticles (80–100 °C) in a acetonitrile mixture (10 mL) containing 3.0×10^{-4} mol dm^{-3} of **Mes–Acr$^+$–COOH** and **Acr$^+$–COOH** for 12 h, respectively. After adsorbing **Mes–Acr$^+$–COOH** and **Acr$^+$–COOH**, the TiO_2 nanoparticles were filtered, and subsequent washing with acetonitrile and drying gave **Mes–Acr$^+$–COO–TiO$_2$** and **Acr$^+$–COO–TiO$_2$**. The dye molecule was completely desorbed from the TiO_2 particles into solution by immersing the TiO_2 nanoparticles modified with the dye moieties in methanol overnight. The amounts of **Mes–Acr$^+$–COOH** and **Acr$^+$–COOH** adsorbed on TiO_2 nanoparticles relative to the total weight were determined as 1.5×10^{-5} and 1.5×10^{-5} mol g^{-1}, respectively.

Electrophoretic deposition of composite clusters on the electrode

C_{60} is soluble in nonpolar solvents such as toluene. In mixed solvents (acetonitrile–toluene), however, it aggregates to form large clusters of diameter 100–300 nm.[25] The C_{60} cluster and TiO_2 nanoparticles were electrophoretically deposited onto SnO_2 films under applied voltage as reported previously.[23–25]

Nanostructured SnO_2 films were cast on an optically transparent electrode (OTE) by applying a dilute (1–2%) colloidal solution (Alfa Chemicals), followed by annealing the dried film at 673 K. Details about the electrode preparation and its properties have been described elsewhere.[26] These films are highly porous and electrochemically active for the conduction of charges across the film. The SnO_2 film electrode (OTE/SnO_2) and an OTE plate were introduced in a 1 cm path length cuvette and they were connected to positive and negative terminals of the power supply, respectively. A known amount ($\sim$2 mL) of C_{60}, **Mes–Acr$^+$–COO–TiO$_2$**, or the mixed cluster suspension in acetonitrile–toluene (3 : 1, v/v) was transferred immediately after the ultrasonication to a 1 cm cuvette in which two electrodes (viz., OTE/SnO_2 and OTE) were kept at a distance of $\sim$6 mm using a Teflon spacer. A dc voltage (500 V) was applied for 2 min between these two electrodes using a Fluke 415 power supply. The deposition of the film could be visibly seen as the solution became colorless, with simultaneous brown coloration of the SnO_2/OTE electrode. The SnO_2/OTE electrode coated with mixed **Mes–Acr$^+$–COO–TiO$_2$** and C_{60} clusters is referred to as OTE/SnO_2/(**Mes–Acr$^+$–COO–TiO$_2$** + C_{60})$_n$.

SnO_2 nanocrystallite films were modified with **Mes–Acr$^+$–COOH** (denoted as OTE/SnO_2/**Mes–Acr$^+$–COOH**) as follows.
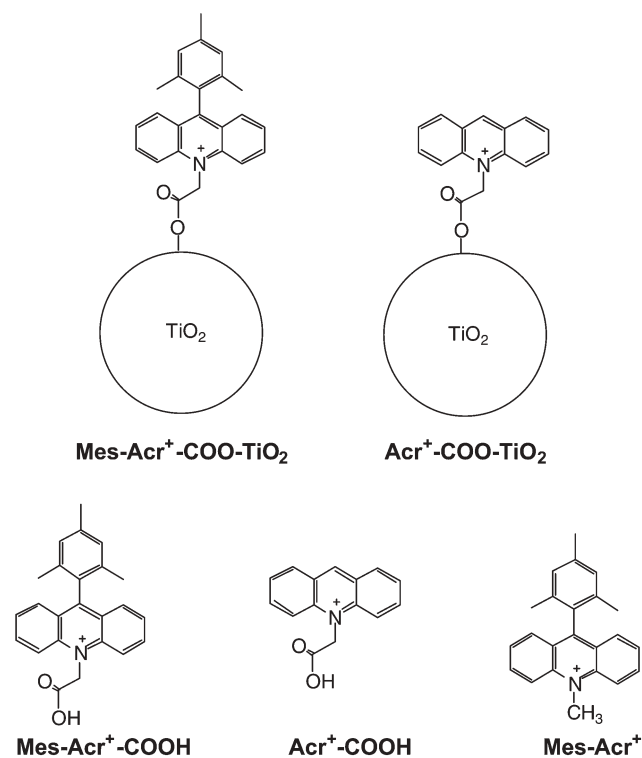

Fig. 1 TiO_2 nanoparticles modified with 9-mesityl-10-carboxymethylacridinium ion and 10-carboxymethylacridinium ion, and the reference compounds employed in this study.

The synthesized dyad (**Mes–Acr⁺–COOH**) was adsorbed by immersing OTE/SnO₂ electrode in a 2×10^{-3} mol dm^{-3} ethanol solution overnight to prepare a OTE/SnO₂/**Mes–Acr⁺–COOH** electrode. In order to remove the adsorbed water from the SnO₂ surface, the films were heated to 80 °C before the immersion. TiO₂ nanocrystallite films modified with **Mes–Acr⁺–COOH** (denoted as OTE/TiO₂/**Mes–Acr⁺–COOH**) are described in the ESI.†

The UV-visible spectra were recorded on a Shimadzu 3101 spectrophotometer. Images were recorded using a Hitachi H600 transmission electron microscope. The morphology of the mesoporous electrodes was characterized by a scanning electron micrograph (SEM; JEOL, JSM-6700FE). The SEM was operated with an accelerating voltage of 10 kV.

Photoelectrochemical measurements

Photoelectrochemical measurements were performed using a standard three-compartment cell consisting of a working electrode and Pt wire gauze counter electrode and saturated calomel reference electrode (SCE). All photoelectrochemical measurements were carried out in acetonitrile containing 0.5 mol dm^{-3} NaI and 0.01 mol dm^{-3} I₂ with a Keithley model 617 programmable electrometer. A collimated light beam from a 150 W Xenon lamp with a 400 nm cut-off filter was used for excitation of the composite cluster films cast on SnO₂ electrodes. A Bausch and Lomb high intensity grating monochromator was introduced into the path of the excitation beam for selecting wavelength. A Princeton Applied Research (PAR) model 173 potentiostat and Model 175 universal programmer were used for recording I–V characteristics.

Transient absorption measurements

Nanosecond laser flash photolysis experiments were performed using a Spectra Physics model PR0230 laser system (355 nm, 10 ns pulse width, 40 mJ per pulse). The laser output was suitably attenuated to about 20 mJ per pulse and defocused to minimize the multiphoton process. The measurements were performed in a rectangular quartz cell of 6 mm path length with a right angle configuration between the direction of laser excitation and analyzing light. The photomultiplier output was digitized with a LeCroy LC-574A programmable digitizer. A typical experiment consisted of a series of 5 replicate shots/single measurements.

Results and discussion

Preparation of the composite cluster film composed of Mes–Acr⁺–COO–TiO₂ and C₆₀ by electrophoretic deposition

TiO₂ nanoparticles were electrophoretically deposited onto the electrode in suspended solution.[24] In contrast, C₆₀ is soluble in nonpolar solvents such as toluene, but less so in polar solvents such as acetonitrile.[25] By the proper choice of a mixture of polar and nonpolar solvents, we can achieve control in the form of aggregation of C₆₀ nanoclusters. Unless otherwise noted, we maintained a final solvent ratio of 3 : 1 (v/v) acetonitrile–toluene to prepare C₆₀ nanoclusters. Detail information of the C₆₀ nanoclusters is described elsewhere.[25] A mixed cluster suspension of **Mes–Acr⁺–COO–TiO₂** and C₆₀

was prepared in the total concentration range from 0.025 to 0.13 mmol dm^{-3} (molecular ratio of **Mes–Acr⁺** to C₆₀ = 1 : 5) in acetonitrile–toluene (3 : 1, v/v).

As shown earlier,[23] clusters suspended in acetonitrile–toluene mixed solvent can be assembled electrophoretically as thin films on a conducting glass electrode surface. A similar electrodeposition approach was adopted to prepare films of (**Mes–Acr⁺–COO–TiO₂** + C₆₀)ₙ on nanostructured SnO₂ films cast on an optically conducting glass electrode. Upon application of the DC electric field of 500 V between OTE/SnO₂ and OTE electrodes which were immersed parallel in a mixed acetonitrile–toluene (3 : 1, v/v) solution containing (**Mes–Acr⁺–COO–TiO₂** + C₆₀)ₙ clusters, we achieved deposition of mixed clusters on a nanostructured SnO₂ electrode. As the deposition continued, we could visually observe discoloration of the solution and coloration of the electrode that was connected to the positive terminal of the dc power supply.

Fig. 2a shows that the absorption spectrum of the OTE/SnO₂/(**Mes–Acr⁺–COO–TiO₂** + C₆₀)ₙ electrode prepared using different precursor concentrations of **Mes–Acr⁺–COO–TiO₂** and C₆₀ in an acetonitrile–toluene (3 : 1, v/v) mixture. Note that the mixed clusters were first prepared using different amounts of **Mes–Acr⁺–COO–TiO₂** and C₆₀ to maintain their molar ratio as 1 : 5. An increase in the absorbance of the OTE/SnO₂/(**Mes–Acr⁺–COO–TiO₂** + C₆₀)ₙ electrode in the visible and near-infrared regions is clearly observed, in contrast with those of individual component: OTE/SnO₂/(**Mes–Acr⁺–COO–TiO₂**)ₙ (Fig. 2b) and OTE/SnO₂/(C₆₀)ₙ (Fig. 2c), which were prepared under the same experimental conditions. In addition, the spectrum of the OTE/SnO₂/(**Mes–Acr⁺–COO–TiO₂**)ₙ film has much broader as well as higher absorption than that of the monolayer film, OTE/SnO₂/**Mes–Acr⁺–COOH** (Fig. 2d). This indicates that the multilayer film of **Mes–Acr⁺–COO–TiO₂** using an electrophoretic deposition method exhibits a high absorption property in all the visible regions. This broad absorption of OTE/SnO₂/(**Mes–Acr⁺–COO–TiO₂**)ₙ may be
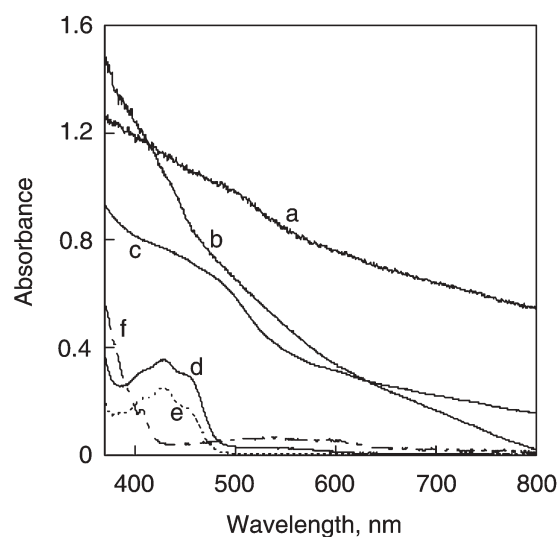

Fig. 2 Absorption spectra of (a) OTE/SnO₂/(**Mes–Acr⁺–COO–TiO₂** + C₆₀)ₙ, (b) OTE/SnO₂/(**Mes–Acr⁺–COO–TiO₂**)ₙ, (c) OTE/SnO₂/(C₆₀)ₙ, (d) OTE/SnO₂/**Mes–Acr⁺–COOH**, (e) **Mes–Acr⁺–COOH** in acetonitrile (4.0×10^{-5} M), and (f) C₆₀ in toluene (1.5×10^{-5} M).

ascribed to a strong interaction in the molecular assembly.[27] Furthermore, broader wavelength absorption in the OTE/ SnO_2/(**Mes–Acr**$^+$**–COO–TiO**$_2$ + **C**$_{60}$)$_n$ film relative to those in the OTE/SnO_2/(**Mes–Acr**$^+$**–COO–TiO**$_2$)$_n$ and OTE/SnO_2/ (**C**$_{60}$)$_n$ films may be diagnostic of a charge-transfer (CT) absorption band between the **Mes–Acr**$^+$ moiety and fullerene since a similar broad absorption, which is characteristic of an intermolecular CT band,[28] is also observed in solution (see the ESI†).

Morphology of OTE/SnO_2/(Mes–Acr$^+$–COO–TiO$_2$ + C$_{60}$)$_n$

Scanning electron microscopy (SEM) was used to evaluate the morphology of the OTE/SnO_2/(**Mes–Acr**$^+$**–COO–TiO**$_2$ + **C**$_{60}$)$_n$ film and the reference film (OTE/SnO_2/(**C**$_{60}$)$_n$), as shown in Fig. 3. The OTE/SnO_2/(**Mes–Acr**$^+$**–COO–TiO**$_2$ + **C**$_{60}$)$_n$ film is composed of closely packed clusters about 20–100 nm in size with a networked structure. This structure may result from a supramolecular interaction between **Mes–Acr**$^+$**–COO–TiO**$_2$ and C_{60} in the TiO_2 nanoparticle matrix. On the other hand, the OTE/SnO_2/(**C**$_{60}$)$_n$ films contain large (100–300 nm) nanoclusters, in contrast to those in the OTE/SnO_2/(**Mes–Acr**$^+$**–COO–TiO**$_2$ + **C**$_{60}$)$_n$ film. This cluster size is in good agreement with our previous AFM images.[25a] Based on these SEM images, we can conclude that TiO_2 nanoparticles play an important role in cluster formation on the films.

Light energy conversion properties

Photocurrent measurements were performed using the OTE/SnO_2/(**Mes–Acr**$^+$**–COO-TiO**$_2$ + **C**$_{60}$)$_n$ electrode as a
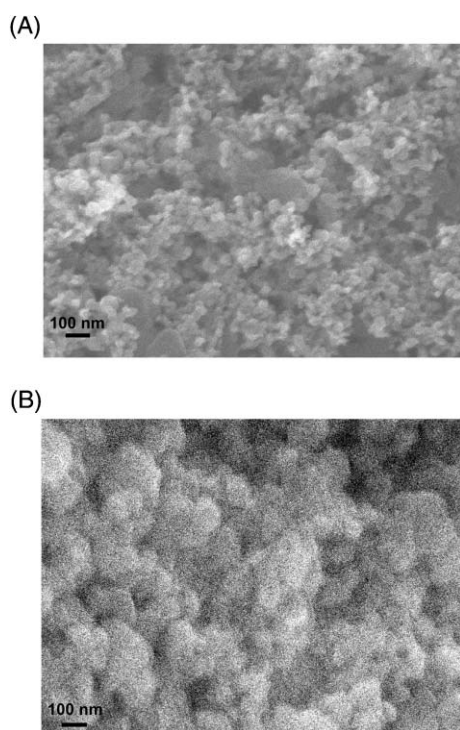
photoanode in acetonitrile containing NaI (0.5 mol dm^{-3}) and I_2 (0.01 mol dm^{-3}), which act as redox electrolyte, and a Pt gauge counter electrode. The photovoltage and photo-current responses recorded following the excitation of the OTE/SnO_2/(**Mes–Acr**$^+$**–COO–TiO**$_2$ + **C**$_{60}$)$_n$ electrode in the visible light region ($\lambda > 400$ nm) are shown in Fig. 4A and B, respectively. The photocurrent response is prompt, steady and reproducible during repeated on/off cycles of the visible light illumination. The short circuit photocurrent density (I_{sc}) is 0.093 mA cm^{-2}, and the open circuit voltage (V_{oc}) is 200 mV. Blank experiments conducted with OTE/SnO_2 (*i.e.*, by excluding composite clusters (**Mes–Acr**$^+$**–COO–TiO**$_2$ + **C**$_{60}$)$_n$ produced no detectable photocurrent under otherwise the same experimental conditions. These experiments confirmed the important role of the (**Mes–Acr**$^+$**–COO–TiO**$_2$ + **C**$_{60}$)$_n$ assembly in harvesting light energy and also in generating photocurrent during the operation of the photoelectrochemical cell.

The charge separation on the OTE/SnO_2/(**Mes–Acr**$^+$**–COO–TiO**$_2$ + **C**$_{60}$)$_n$ electrode can be further modulated by the application of an electrochemical bias. Fig. 5 shows *I–V* characteristics of the OTE/SnO_2/(**Mes–Acr**$^+$**–COO–TiO**$_2$ + **C**$_{60}$)$_n$ electrode under visible light illumination. The photo-current increases as the applied potential is scanned towards more positive potentials. Increased charge separation and the facile transport of charge carriers under a positive bias are responsible for the enhanced photocurrent generation.[23a] At potentials greater than +0.4 V *vs.* SCE, direct electrochemical oxidation of iodide interferes with the photocurrent measurement.

A series of photocurrent action spectra were recorded in order to evaluate the response of (**Mes–Acr**$^+$**–COO–TiO**$_2$ + **C**$_{60}$)$_n$ clusters towards the photocurrent generation. It should be noted that no net photocurrent is observed through the visible region in the photocurrent action spectrum of TiO_2
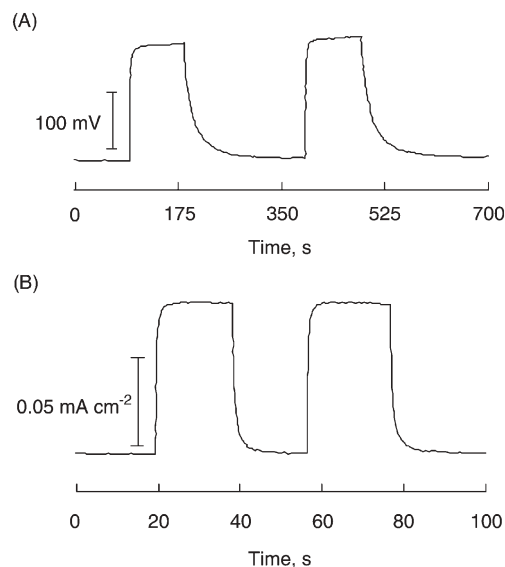

(A)

(B)

Fig. 3 SEM (scanning electron microscopy) images of (A) OTE/SnO_2/ (**Mes–Acr**$^+$**–COO–TiO**$_2$ + **C**$_{60}$)$_n$ ([**Mes–Acr**$^+$] = 0.025 mmol dm^{-3}, [**C**$_{60}$] = 0.13 mmol dm^{-3}) and (B) OTE/SnO_2/(**C**$_{60}$)$_n$ ([**C**$_{60}$] = 0.13 mmol dm^{-3}).

(A)

100 mV

(B)

0.05 mA cm^{-2}

Fig. 4 (A) Photovoltage and (B) photocurrent generation at OTE/ SnO_2/(**Mes–Acr**$^+$**–COO–TiO**$_2$ + **C**$_{60}$)$_n$ ([**Mes–Acr**$^+$] = 0.025 mmol dm^{-3}, [**C**$_{60}$] = 0.13 mmol dm^{-3}) under white light illumination ($\lambda > 400$ nm); electrolyte: 0.5 mol dm^{-3} NaI and 0.01 mol dm^{-3} I_2 in acetonitrile; input power: 6.5 mW cm^{-2}.
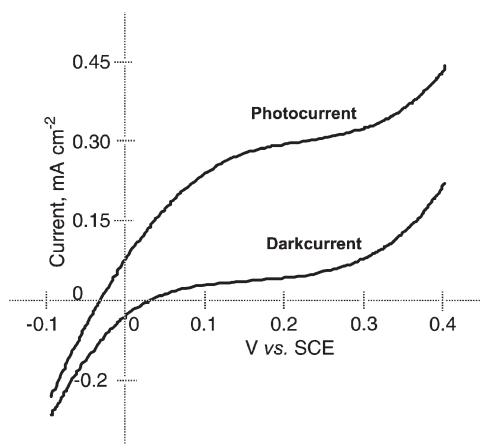
Fig. 5 *I–V* characteristics of OTE/SnO$_2$/(**Mes–Acr$^+$–COO–TiO$_2$** + C$_{60}$)$_n$ ([**Mes–Acr$^+$**] = 0.025 mmol dm^{-3}, [C$_{60}$] = 0.13 mmol dm^{-3}) under white light illumination (λ > 400 nm); electrolyte: 0.5 mol dm^{-3} NaI and 0.01 mol dm^{-3} and I$_2$ in acetonitrile; input power: 6.5 mW cm^{-2}.

nanocrystallites films modified with **Mes–Acr$^+$–COOH** (denoted as OTE/TiO$_2$/**Mes–Acr$^+$–COOH**); see the ESI.† Since the one-electron reduction potential of acridinium ion (**Acr$^+$/Acr$^\bullet$**) (-0.3 V *vs.* NHE) is less negative than the conduction band of TiO$_2$ (-0.5 V *vs.* NHE), electron transfer from **Acr$^\bullet$** to the conduction band of TiO$_2$ is thermodynamically unfavorable. Thus, TiO$_2$ nanoparticles act as materials to organize composite molecules rather than as those to accept electrons. The photocurrent action spectrum of the OTE/SnO$_2$/(**Mes–Acr$^+$–COO–TiO$_2$** + C$_{60}$)$_n$ electrode produced by the electrodeposition of **Mes–Acr$^+$–COO–TiO$_2$** and C$_{60}$ ([**Mes–Acr$^+$**] = 0.025 mmol dm^{-3}, [C$_{60}$] = 0.13 mmol dm^{-3}) is shown in Fig. 6A. The incident photon-to-photocurrent generation efficiency (IPCE) values were calculated by

normalizing the photocurrent values for incident light energy and intensity and using eqn. (1),[23a]

$$\text{IPCE} \ (\%) = 100 \ \times \ 1240 \ \times \ I_{\text{sc}}/(W_{\text{in}} \ \times \ \lambda) \tag{1}$$

where I_{sc} is the short circuit photocurrent (A cm^{-2}), W_{in} is the incident light intensity (W cm^{-2}), and λ is the wavelength (nm).

The maximum IPCE value of OTE/SnO$_2$/**Mes–Acr$^+$–COOH** (spectrum a in Fig. 6A) is only 2% (445 nm), whereas the IPCE value of OTE/SnO$_2$/(Mes–Acr$^+$–COO–TiO$_2$)$_n$ (spectrum b) reaches 5% (480 nm). In addition, the IPCE values of the OTE/SnO$_2$/(**Mes–Acr$^+$–COO–TiO$_2$** + C$_{60}$)$_n$ electrode (spectrum c) are much higher than the sum (spectrum e) of two individual IPCE values of OTE/SnO$_2$/(**Mes–Acr$^+$–COO–TiO$_2$**)$_n$ (spectrum b) and OTE/SnO$_2$/(C$_{60}$)$_n$ (spectrum d) in the visible region. This indicates that the supramolecular complexes formed between **Mes–Acr$^+$** and C$_{60}$ with TiO$_2$ nanoparticles contribute significantly to the efficient photocurrent generation.[23]

In order to further clarify the effect of the supramolecular complex with TiO$_2$ nanoparticles on the photocurrent generation, we compared the photocurrent action spectrum of the OTE/SnO$_2$/(**Mes–Acr$^+$–COO–TiO$_2$** + C$_{60}$)$_n$ electrode with those of OTE/SnO$_2$/(C$_{60}$)$_n$ and OTE/SnO$_2$/(**Mes–Acr$^+$–COO–TiO$_2$**)$_n$ electrodes in a standard three-compartment cell under a bias of 0.2 V *vs.* SCE (Fig. 6B).[23] The photocurrent action spectrum of the OTE/SnO$_2$/(**Mes–Acr$^+$–COO–TiO$_2$** + C$_{60}$)$_n$ electrode shows a maximum IPCE value of 37% at an applied potential of 0.2 V *vs.* SCE (spectrum a in Fig. 6B). Under the same experimental conditions we observe much smaller IPCE values for the single component systems, *viz.*, OTE/SnO$_2$/(C$_{60}$)$_n$ and OTE/SnO$_2$/(**Mes–Acr$^+$–COO–TiO$_2$**)$_n$ (spectra b and c in Fig. 6B, respectively). The IPCE value obtained with the
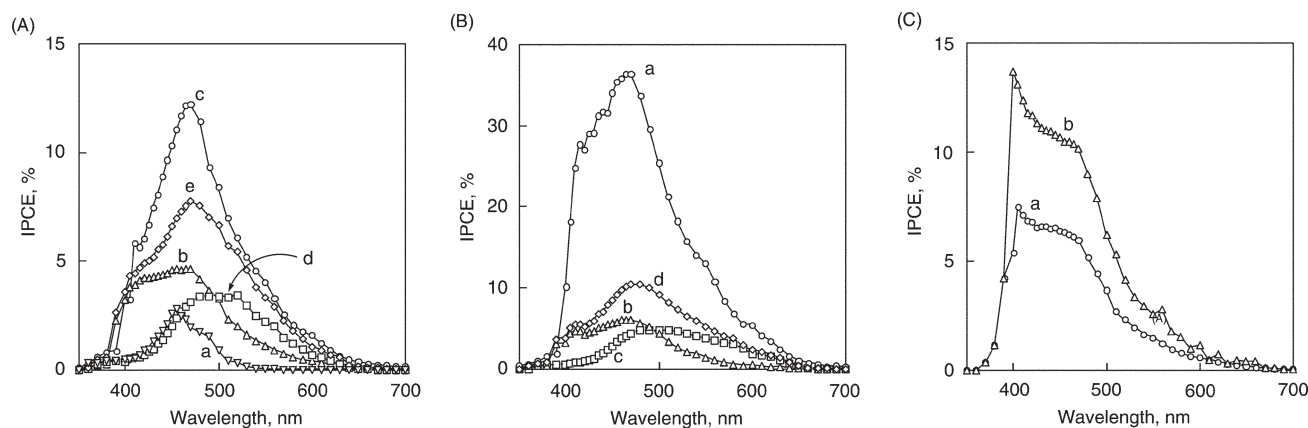
Fig. 6 (A) Photocurrent action spectra (IPCE *vs.* wavelength) of (a) OTE/SnO$_2$/**Mes–Acr$^+$–COOH**, (b) OTE/SnO$_2$/(**Mes–Acr$^+$–COO–TiO$_2$**)$_n$ ([**Mes–Acr$^+$**] = 0.025 mmol dm^{-3}), (c) OTE/SnO$_2$/(**Mes–Acr$^+$–COO–TiO$_2$** + C$_{60}$)$_n$ ([**Mes–Acr$^+$**] = 0.025 mmol dm^{-3}, [C$_{60}$] = 0.13 mmol dm^{-3}), (d) OTE/SnO$_2$/(C$_{60}$)$_n$ ([C$_{60}$] = 0.13 mmol dm^{-3}), and (e) the sum of the IPCE response of OTE/SnO$_2$/(**Mes–Acr$^+$–COO–TiO$_2$**)$_n$ (b) and OTE/SnO$_2$/(C$_{60}$)$_n$ (d) with no applied bias potential. (B) Photocurrent action spectra (IPCE *vs.* wavelength) of (a) OTE/SnO$_2$/(**Mes–Acr$^+$–COO–TiO$_2$** + C$_{60}$)$_n$ ([**Mes–Acr$^+$**] = 0.025 mmol dm^{-3}, [C$_{60}$] = 0.13 mmol dm^{-3}), (b) OTE/SnO$_2$/(**Mes–Acr$^+$–COO–TiO$_2$**)$_n$ ([**Mes–Acr$^+$**] = 0.025 mmol dm^{-3}), (c) OTE/SnO$_2$/(C$_{60}$)$_n$ ([**Mes–Acr$^+$**] = 0.025 mmol dm^{-3}, [C$_{60}$] = 0.13 mmol dm^{-3}), (d) the sum of the IPCE response of OTE/SnO$_2$/(**Mes–Acr$^+$–COO–TiO$_2$**)$_n$ (b) and OTE/SnO$_2$/(C$_{60}$)$_n$ (c) at an applied bias potential of 0.2 V *vs.* SCE. (C) Photocurrent action spectra (IPCE *vs.* wavelength) of (a) OTE/SnO$_2$/(**Acr$^+$–COO–TiO$_2$** + C$_{60}$)$_n$ ([**Acr$^+$**] = 0.025 mmol dm^{-3}, [C$_{60}$] = 0.13 mmol dm^{-3}), with no applied bias potential and (b) OTE/SnO$_2$/(**Acr$^+$–COO–TiO$_2$** + C$_{60}$)$_n$ ([**Acr$^+$**] = 0.025 mmol dm^{-3}, [C$_{60}$] = 0.13 mmol dm^{-3}) at an applied bias potential of 0.2 V *vs.* SCE. Electrolyte: 0.5 mol dm^{-3} NaI and 0.01 mol dm^{-3} and I$_2$ in acetonitrile.

mixed cluster system (37%), *viz.* OTE/SnO$_2$/(**Mes–Acr**$^+$**–COO–TiO$_2$** + C$_{60}$)$_n$ is larger than the sum of two individual IPCE values (~11%). Such enhancement in the photocurrent generation of the composite cluster systems of **Mes–Acr**$^+$**–COO–TiO$_2$** and C$_{60}$ compared with the single component systems may result from interplay between **Mes–Acr**$^+$**–COO–TiO$_2$** and C$_{60}$ in the supramolecular complex.

We have also compared photocurrent action spectra of the OTE/SnO$_2$/(**Acr**$^+$**–COO–TiO$_2$** + C$_{60}$)$_n$ electrode (Fig. 6C), in which the acridinium moiety (**Acr**$^+$) contains no donor moiety, with that of the OTE/SnO$_2$/(**Mes–Acr**$^+$**–COO–TiO$_2$** + C$_{60}$)$_n$ electrode. The maximum IPCE value of the OTE/SnO$_2$/(**Acr**$^+$**–COO–TiO$_2$** + C$_{60}$)$_n$ electrode in standard two (no bias) and three (0.2 V *vs.* SCE) compartment cells (*vide supra*) reached 7 and 14%, respectively. These IPCE values are significantly smaller than those of the OTE/SnO$_2$/(**Mes–Acr**$^+$**–COO–TiO$_2$** + C$_{60}$)$_n$ electrodes (respective values: 13% and 37%). This indicates that photoinduced electron transfer from the donor moiety (**Mes**) to the acceptor moiety (**Acr**$^+$) occurs, followed by electron transfer from the resulting acridinyl radical moiety (**Acr**$^•$) to C$_{60}$ in the supramolecular complex, leading to enhanced photocurrent generation.

Electron transfer in the supramolecular complex

In order to confirm the occurrence of photoinduced electron transfer from the **Mes** moiety to the **Acr**$^+$ moiety and subsequent electron transfer from the resulting acridinyl radical moiety (**Acr**$^•$) to C$_{60}$ in the supramolecular complex, we examined formation of C$_{60}$ radical anion in the nanosecond laser flash photolysis measurements of deoxygenated toluene–acetonitrile (1 : 1, v/v) solution of 9-mesityl-10-methylacridinium ion without carboxylic acid (**Mes–Acr**$^+$)[16] in the presence of C$_{60}$. The time-resolved transient absorption spectra are shown in Fig. 7A, which clearly exhibits a broad absorption band at about 1050 nm. This is diagnostic of formation of C$_{60}$ radical anion upon photoirradiation.[29–31] Thus, electron transfer indeed occurs from the acridinyl radical moiety (**Acr**$^•$) to C$_{60}$, following photoinduced electron transfer from the **Mes** moiety to the singlet excited state of **Acr**$^+$ moiety of **Mes–Acr**$^+$ to produce the electron-transfer state, **Mes**$^{•+}$**–Acr**$^•$, which is known to have an extremely long lifetime.[16] The absorption time profile of the composite cluster (**Mes–Acr**$^+$ dyad and C$_{60}$) in deoxygenated toluene–acetonitrile (1 : 1) recorded at 1050 nm is shown in Fig. 7B.[31] The observed second-order decay kinetics (inset of Fig. 7B) corresponds to back electron transfer from C$_{60}$$^{•−}$ to the **Mes**$^{•+}$ moiety of **Mes**$^{•+}$**–Acr**$^+$, affording the second-order rate constant of the back electron transfer (k_{bet} = 2.9 × 10^9 dm^3 mol^{-1} s^{-1}).

Photocurrent generation mechanism

Mechanisms of the photocurrent generation of OTE/SnO$_2$/(C$_{60}$)$_n$, OTE/SnO$_2$/(**Mes–Acr**$^+$**–COO–TiO$_2$**)$_n$, and OTE/SnO$_2$/(**Mes–Acr**$^+$**–COO–TiO$_2$** + C$_{60}$)$_n$ electrodes are summarized in Schemes 1, 2 and 3, respectively. In the case of the OTE/SnO$_2$/(C$_{60}$)$_n$ electrode (Scheme 1), photoinduced electron transfer between iodide ion and the excited state of C$_{60}$ clusters is the first step in photocurrent generation.[23a,25b,32] The reduced C$_{60}$ then injects electrons into SnO$_2$ nanocrystallites. Such a
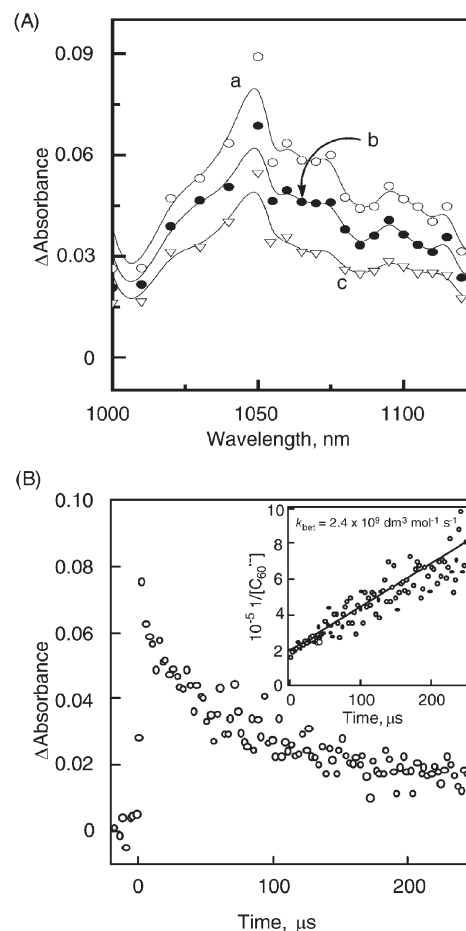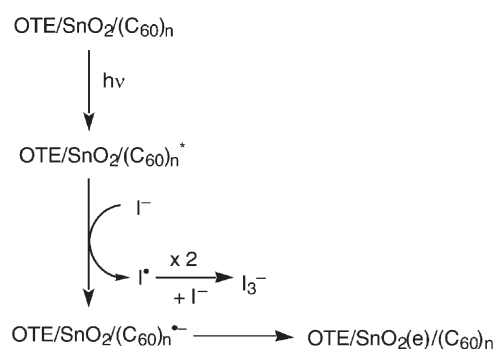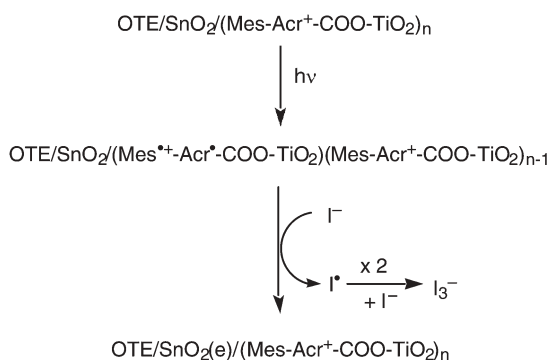

Fig. 7 (A) Transient absorption spectra of **Mes–Acr**$^+$ (7.5 × 10^{-6} mol dm^{-3}) with C$_{60}$ (7.5 × 10^{-6} mol dm^{-3}) in a deoxygenated toluene–acetonitrile (1 : 1) mixture at 298 K taken at (a) 20 µs, (b) 50 µs and (c) 100 µs after laser pulse excitation at 355 nm. (B) Decay profile of absorbance at 1050 nm. Inset: second-order plot.

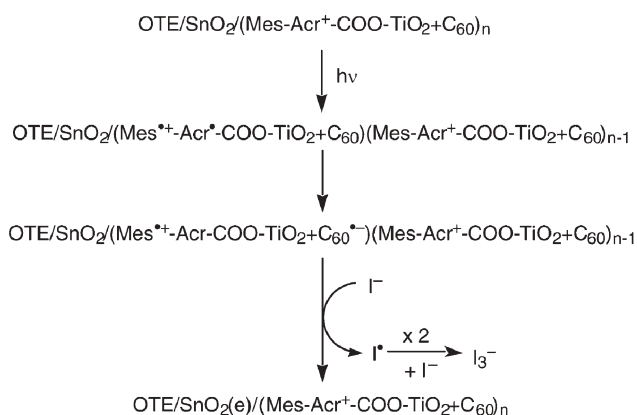**Scheme 1** Photocurrent generation diagram of the OTE/SnO$_2$/(C$_{60}$)$_n$ electrode.

mechanism involving generation of electroactive species (C$_{60}$ anion in the present case) is commonly operative in photogalvanic-type solar cells.[23,25] In the case of the OTE/SnO$_2$/(**Mes–Acr**$^+$**–COO–TiO$_2$**)$_n$ electrode (Scheme 2), however, the photocurrent generation is initiated by photoinduced electron transfer in **Mes–Acr**$^+$ to produce **Mes**$^{•+}$**–Acr**$^•$. The reduced acridinium ion (**Acr**$^•$; $E°$(**Acr**$^+$/**Acr**$^•$) = −0.3 V *vs.* NHE)[16]

This journal is © The Royal Society of Chemistry 2005

J. Mater. Chem., 2005, **15**, 372–380 | 377

OTE/SnO₂/(Mes-Acr⁺-COO-TiO₂)ₙ
↓ hν
OTE/SnO₂/(Mes•⁺-Acr•-COO-TiO₂)(Mes-Acr⁺-COO-TiO₂)ₙ₋₁
↓ I⁻ → I• —x2, +I⁻→ I₃⁻
OTE/SnO₂(e)/(Mes-Acr⁺-COO-TiO₂)ₙ

Scheme 2 Photocurrent generation diagram of the OTE/SnO₂/(**Mes–Acr⁺–COO–TiO₂**)ₙ electrode.

injects electrons into the conduction band of SnO₂ ($E° = 0$ V vs. NHE),[23a] whereas the oxidized mesityl moiety (**Mes**•⁺; $E°$(**Mes/Mes**•⁺) = 2.0 V vs. NHE)[16] undergoes the electron-transfer reduction with iodide ion ($E°$(I₃⁻/I⁻) = 0.5 V vs. NHE)[23a] in the electrolyte solution.

In the case of the OTE/SnO₂/(**Mes–Acr⁺–COO–TiO₂** + C₆₀)ₙ electrode (Scheme 3), the long lifetime of the electron-transfer state (**Mes**•⁺–**Acr**•) ensures efficient electron-transfer from **Acr**• to C₆₀ (C₆₀/C₆₀•⁻ = −0.2 V vs. NHE)[23a] to produce C₆₀ radical anion (*vide supra*). The reduced C₆₀ clusters inject electrons into the conduction band of SnO₂, whereas the oxidized mesityl moiety (**Mes**•⁺) undergoes the electron-transfer reduction with iodide ion in the electrolyte. The effect of C₆₀ on the enhanced photocurrent generation cannot be ascribed to the thermodynamics of electron injection process. The enhanced IPCE value at the absorption band due to the **Acr**⁺ moiety by the presence of C₆₀ results from fast self-exchange electron transfer between C₆₀•⁻ and C₆₀,[29,33] which leads to efficient photocurrent generation, since the singlet excited state of the **Acr**⁺ moiety is mostly quenched by the **Mes** moiety, followed by electron transfer from the resulting **Acr**• moiety to C₆₀. Enhanced IPCE values of the OTE/SnO₂/(**Mes–Acr⁺–COO–TiO₂** + C₆₀)ₙ electrode (spectrum c in Fig. 6A) compared to the sum of two IPCE values of the corresponding single component systems (spectrum e in Fig. 6A) in the long wavelength region over 500 nm may

OTE/SnO₂/(Mes-Acr⁺-COO-TiO₂+C₆₀)ₙ
↓ hν
OTE/SnO₂/(Mes•⁺-Acr•-COO-TiO₂+C₆₀)(Mes-Acr⁺-COO-TiO₂+C₆₀)ₙ₋₁
↓
OTE/SnO₂/(Mes•⁺-Acr-COO-TiO₂+C₆₀•⁻)(Mes-Acr⁺-COO-TiO₂+C₆₀)ₙ₋₁
↓ I⁻ → I• —x2, +I⁻→ I₃⁻
OTE/SnO₂(e)/(Mes-Acr⁺-COO-TiO₂+C₆₀)ₙ

Scheme 3 Photocurrent generation diagram of the OTE/SnO₂/(**Mes–Acr⁺–COO–TiO₂** + C₆₀)ₙ electrode.
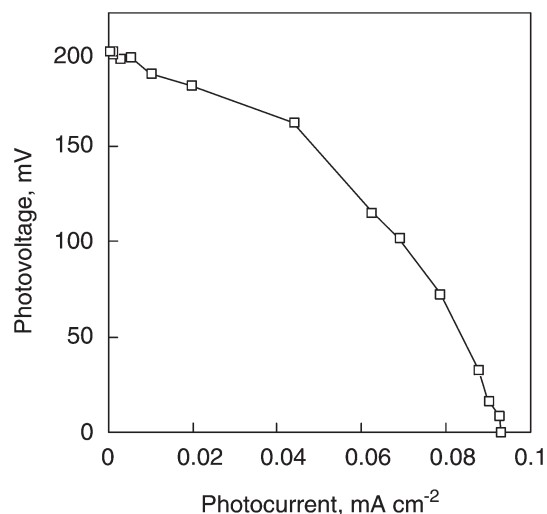
Fig. 8 Power characteristics of OTE/SnO₂/(**Mes–Acr⁺–COO–TiO₂** + C₆₀)ₙ ([**Mes–Acr⁺**] = 0.025 mmol dm⁻³, [C₆₀] = 0.13 mmol dm⁻³) under white light illumination ($\lambda > 400$ nm); electrolyte: 0.5 mol dm⁻³ NaI and 0.01 mol dm⁻³ and I₂ in acetonitrile; input power: 6.5 mW cm⁻².

result from charge-transfer (CT) interaction between the **Mes** (donor) moiety of **Mes–Acr⁺–COOH** and C₆₀ clusters (see ESI†).

Power conversion efficiency

We have also determined the power conversion efficiency (η) of the photoelectrochemical cell by varying the load resistance (Fig. 8). Power conversion efficiency, η, can be calculated from eqn. (2),[23a]

$$\eta = ff \times I_{sc} \times V_{oc}/W_{in} \qquad (2)$$

where the fill factor (*ff*) is defined as $ff = P_{max}/(V_{oc} \times I_{sc})$, P_{max} is the maximum power output of the cell, V_{oc} is open circuit photovoltage, and I_{sc} is the short circuit photocurrent. A decrease in the photovoltage accompanied by an increase in the photocurrent was observed by decreasing the load resistance (Fig. 8). The *ff* value of the (**Mes–Acr⁺–COO–TiO₂** + C₆₀)ₙ electrode was determined as 0.38. Net power conversion efficiency obtained for the same cell was 0.11% at an input power of 6.5 mW cm⁻².[34]

Conclusion

We have successfully constructed a supramolecular photovoltaic composed of composite molecular nanocluster assemblies of fullerene and a simple molecular dyad (**Mes–Acr⁺–COOH**) with an extremely long lifetime and a high energy of the electron-transfer state, which is efficiently organized using TiO₂ nanoparticles. A remarkable improvement in the photoelectrochemical properties of the composite of **Mes–Acr⁺–COOH** and C₆₀ nanoclusters has been achieved, compared with the corresponding single component systems (OTE/SnO₂/(C₆₀)ₙ and OTE/SnO₂/(**Mes–Acr⁺–COO–TiO₂**)ₙ), due to the effective organization of the supramolecular complex on TiO₂

nanoparticles, the extremely long lifetime of the electron-transfer state of **Mes–Acr$^+$–COOH**, and efficient electron transfer from **Acr˙** to C_{60}.

Acknowledgements

Taku Hasobe,[abc] **Shigeki Hattori,**[ab] **Prashant V. Kamat,**[c] **Yuji Wada**[a] **and Shunichi Fukuzumi**[*ab]

[a]*Department of Material and Life Science, Graduate School of Engineering, Osaka University, Suita, Osaka 565-0871, Japan. E-mail: fukuzumi@chem.eng.osaka-u.ac.jp*
[b]*CREST, Japan Science and Technology Agency, Suita, Osaka 565-0871, Japan*
[c]*Radiation Laboratory and Department of Chemical & Biomolecular Engineering, University of Notre Dame, Notre Dame, Indiana 46556, USA*

References

1 (a) G. M. Whitesides and B. Grzybowski, *Science*, 2002, **295**, 2418; (b) G. M. Whitesides, J. P. Mathias and C. T. Seto, *Science*, 1991, **254**, 1312; (c) N. B. Bowden, M. Weck, I. S. Choi and G. M. Whitesides, *Acc. Chem. Res.*, 2001, **34**, 231; (d) D. Philip and J. F. Stoddart, *Angew. Chem., Int. Ed.*, 1996, **35**, 1155; (e) P. Ball, *The Self-Made Tapestry: Pattern Formation in Nature*, Oxford University Press, Oxford, 1999.

2 (a) J.-M. Lehn, *Science*, 2002, **295**, 2400; (b) L. R. MacGillivray and J. L. Atwood, *Nature*, 1997, **389**, 469; (c) C. M. Drain, R. Fischer, E. G. Nolen and J.-M. Lehn, *J. Chem. Soc., Chem. Commun.*, 1993, 243; (d) M. M. Conn and J. Rebek, Jr., *Chem. Rev.*, 1997, **97**, 1647.

3 (a) S. C. Zimmerman, F. Zeng, D. E. C. Reichert and S. V. Kolotuchin, *Science*, 1996, **271**, 1095; (b) R. H. Vreekamp, J. P. M. van Duynhoven, M. Hubert, W. Verboom and D. N. Reinhoudt, *Angew. Chem., Int. Ed. Engl.*, 1996, **35**, 1215; (c) O. Ikkala and G. T. Brinke, *Science*, 2002, **295**, 2407; (d) M. Fujita, *Acc. Chem. Res.*, 1999, **32**, 53.

4 (a) U. Siggel, U. Bindig, C. Endish, T. Komatsu, E. Tsuchida, J. Voigt and J.-H. Fuhrhop, *Ber. Bunsen-Ges. Phys. Chem.*, 1996, **12**, 2070; (b) J.-H. Fuhrhop, U. Bindig and U. Siggel, *J. Am. Chem. Soc.*, 1993, **115**, 11036; (c) S. Santoso, W. Hwang, H. Hartman and S. Zhang, *Nano Lett.*, 2002, **2**, 687; (d) T. Yokoyama, S. Yokoyama, T. Kamikado, Y. Okuno and S. Mashiko, *Nature*, 2001, **413**, 619; (e) X. Qiu, C. Wang, S. Yin, Q. Zeng, B. Xu and C. Bai, *J. Phys. Chem. B*, 2000, **104**, 3570.

5 (a) J. R. Fredericks and A. D. Hamilton, 'Hydrogen Bonding Control of Molecular Self-Assembly: Recent Advances in Design, Synthesis, and Analysis', in *Comprehensive Supramolecular Chemistry*, ed. J.-P. Sauvage and M. W. Hosseini, Pergamon Press, Oxford, 1996, vol. IX, ch. 16; (b) T. van der Boom, R. T. Hayes, Y. Zhao, P. J. Bushard, E. A. Weiss and M. R. Wasielewski, *J. Am. Chem. Soc.*, 2002, **124**, 9582; (c) B. Gong, C. Zheng, E. Skrzypczak-Jankun and J. Zhu, *Org. Lett.*, 2000, **2**, 3273; (d) N. D. McClenaghan, C. Absalon and D. M. Bassani, *J. Am. Chem. Soc.*, 2003, **125**, 13004; (e) C. Pagba, G. Zordan, E. Galoppini, E. L. Piatnitski, S. Hore, K. Deshayes and P. Piotrowiak, *J. Am. Chem. Soc.*, 2004, **126**, 9888.

6 (a) *Anoxygenic Photosynthetic Bacteria*, eds. R. E. Blankenship, M. T. Madigan and C. E. Bauer, Kluwer Academic Publishers, Dordecht, 1995; (b) *The Photosynthetic Reaction Center*, eds. J. Deisenhofer and J. R. Norris, Academic Press, San Diego, 1993;

(c) G. Mcdermott, S. M. Prince, A. A. Freer, A. M. Hawthornthwaite-Lawless, M. Z. Papiz, R. J. Cogdell and N. W. Isaacs, *Nature*, 1995, **374**, 517; (d) U. Ermler, G. Fritzsch, S. K. Buchanan and H. Michel, *Structure*, 1994, **2**, 925; (e) J. Deisenhofer and H. Michel, *Science*, 1989, **245**, 1463.

7 (a) D. Holten and C. Kirmaier, *Photosynth. Res.*, 1987, **13**, 225; (b) A. J. Hoff, *Photochem. Photobiol.*, 1986, **43**, 727.

8 D. Gust, T. A. Moore and A. L. Moore, in *Electron Transfer in Chemistry*, ed. V. Balzani, Wiley-VCH, Weinheim, 2001, vol. 3, pp. 272–336.

9 (a) K. D. Jordan and M. N. Paddon-Row, *Chem. Rev.*, 1992, **92**, 395; (b) J. W. Verhoeven, *Adv. Chem. Phys.*, 1999, **106**, 603.

10 (a) A. Harriman and J.-P. Sauvage, *Chem. Soc. Rev.*, 1996, **25**, 41; (b) M. R. Wasielewski, *Chem. Rev.*, 1992, **92**, 435.

11 (a) S. Fukuzumi and H. Imahori, in *Electron Transfer in Chemistry*, ed. V. Balzani, Wiley-VCH, Weinheim, 2001, vol. 2, pp. 927–975; (b) S. Fukuzumi, and D. M. Guldi, in *Electron Transfer in Chemistry*; ed. V. Balzani, Wiley-VCH, Weinheim, 2001, vol. 2, pp. 270–337.

12 (a) H. Imahori, D. M. Guldi, K. Tamaki, Y. Yoshida, C. Luo, Y. Sakata and S. Fukuzumi, *J. Am. Chem. Soc.*, 2001, **123**, 6617; (b) D. M. Guldi, H. Imahori, K. Tamaki, Y. Kashiwagi, H. Yamada, Y. Sakata and S. Fukuzumi, *J. Phys. Chem. A*, 2004, **108**, 541; (c) D. Gust and T. A. Moore, in *The Porphyrin Handbook*, ed. K. M. Kadish, K. M. Smith and R. Guilard, Academic Press, San Diego, CA, 2000, vol. 8, pp. 153–190; (d) D. Gust, T. A. Moore and A. L. Moore, *Acc. Chem. Res.*, 2001, **34**, 40.

13 (a) H. Imahori and S. Fukuzumi, *Adv. Mater.*, 2001, **13**, 1197; (b) H. Yamada, H. Imahori, Y. Nishimura, I. Yamazaki, T. K. Ahn, S. K. Kim, D. Kim and S. Fukuzumi, *J. Am. Chem. Soc.*, 2003, **125**, 9129; (c) H. Imahori, H. Norieda, H. Yamada, Y. Nishimura, I. Yamazaki, Y. Sakata and S. Fukuzumi, *J. Am. Chem. Soc.*, 2001, **123**, 100.

14 (a) M. Lahav, T. Gabriel, A. N. Shipway and I. Willner, *J. Am. Chem. Soc.*, 1999, **121**, 258; (b) M. Lahav, V. Heleg-Shabtai, J. Wasserman, E. Katz, I. Willner, H. Dürr, Y.-Z. Hu and S. H. Bossmann, *J. Am. Chem. Soc.*, 2000, **122**, 11480.

15 J.-F. Eckert, J.-F. Nicoud, J.-F. Nierengarten, S.-G. Liu, L. Echegoyen, F. Barigelletti, N. Armaroli, L. Ouali, V. Krasnikov and G. Hadziioannou, *J. Am. Chem. Soc.*, 2000, **122**, 7467.

16 S. Fukuzumi, H. Kotani, K. Ohkubo, S. Ogo, N. V. Tkachenko and H. Lemmetyinen, *J. Am. Chem. Soc.*, 2004, **126**, 1600.

17 (a) A. Hagfeldt and M. Grätzel, *Chem. Rev.*, 1995, **95**, 49; (b) A. Hagfeldt and M. Grätzel, *Acc. Chem. Res.*, 2000, **33**, 269; (c) M. Grätzel, *Nature*, 2001, **414**, 338; (d) C. A. Bignozzi, R. Argazzi and C. J. Kleverlaan, *Chem. Soc. Rev.*, 2000, **29**, 87.

18 (a) P. Bonhôte, J.-E. Moser, R. Humphry-Baker, N. Vlachopoulos, S. M. Zakeeruddin, L. Walder and M. Grätzel, *J. Am. Chem. Soc.*, 1999, **121**, 1324; (b) A. Hagfeldt and M. Grätzel, *Acc. Chem. Res.*, 2000, **33**, 269; (c) A. Shah, P. Torres, R. Tscharner, N. Wyrsch and H. Keppner, *Science*, 1999, **285**, 692.

19 (a) B. O'Regan and M. Grätzel, *Nature*, 1991, **353**, 737; (b) U. Bach, D. Lupo, P. Comte, J. E. Moser, F. Weissörtel, J. Salbeck, H. Spreitzer and M. Grätzel, *Nature*, 1998, **395**, 583; (c) R. Cinnsealach, G. Boschloo, S. N. Rao and D. Fitzmaurice, *Sol. Energy Mater. Sol. Cells*, 1999, **55**, 215; (d) P. Peumans, S. Uchida and S. R. Forrest, *Nature*, 2003, **425**, 158.

20 (a) D. Zhang, T. Yoshida and H. Minoura, *Chem. Lett.*, 2002, 874; (b) D. Zhang, T. Yoshida and H. Minoura, *Adv. Mater.*, 2003, **15**, 814.

21 (a) S. E. Shaheen, C. J. Brabec, N. S. Sariciftci, F. Padinger, T. Fromherz and J. C. Hummelen, *Appl. Phys. Lett.*, 2001, **78**, 841; (b) F. Padinger, R. S. Rittberger and N. S. Sariciftci, *Adv. Funct. Mater.*, 2003, **13**, 85.

22 (a) M. Granström, K. Petrisch, A. C. Arias, A. Lux, M. R. Andersson and R. H. Friend, *Nature*, 1998, **395**, 257; (b) J. J. M. Halls, C. A. Walsh, N. C. Greenham, E. A. Marseglia, R. H. Friend, S. C. Moratti and A. B. Holmes, *Nature*, 1995, **376**, 498; (c) G. Yu, J. Gao, J. C. Hummelen, F. Wudl and A. J. Heeger, *Science*, 1995, **270**, 1789.

23 (a) T. Hasobe, H. Imahori, S. Fukuzumi and P. V. Kamat, *J. Phys. Chem. B*, 2003, **107**, 12105; (b) T. Hasobe, H. Imahori, P. V. Kamat and S. Fukuzumi, *J. Am. Chem. Soc.*, 2003, **125**, 14962; (c)

T. Hasobe, Y. Kashiwagi, M. A. Absalom, J. Sly, K. Hosomizu, M. A. Crossley, H. Imahori, P. V. Kamat and S. Fukuzumi, *Adv. Mater.*, 2004, **16**, 975; (*d*) T. Hasobe, S. Hattori, H. Kotani, K. Ohkubo, K. Hosomizu, H. Imahori, P. V. Kamat and S. Fukuzumi, *Org. Lett.*, 2004, **6**, 3103.

24 (*a*) Y. Matsumoto, M. Noguchi, T. Matsunaga, K. Kamada, M. Koinuma and S. Yamada, *Electrochemistry*, 2001, **69**, 314; (*b*) T. Miyasaka, Y. Kijitori, T. N. Murakami, M. Kimura and S. Uegusa, *Chem. Lett.*, 2002, 1250; (*c*) D. Matthews, A. Kay and M. Grätzel, *Aust. J. Chem.*, 1994, **47**, 1869; (*d*) D. Xu, Y. Xu, D. Chen, G. Guo, L. Gui and Y. Tang, *Adv. Mater.*, 2000, **12**, 520.

25 (*a*) S. Barazzouk, S. Hotchandani and P. V. Kamat, *Adv. Mater.*, 2001, **13**, 1614; (*b*) P. V. Kamat, S. Barazzouk, K. G. Thomas and S. Hotchandani, *J. Phys. Chem. B*, 2000, **104**, 4014.

26 I. Bedja, S. Hotchandani and P. V. Kamat, *J. Phys. Chem.*, 1994, **98**, 4133.

27 T. Hasobe, H. Imahori, S. Fukuzumi and P. V. Kamat, *J. Mater. Chem.*, 2003, **13**, 2315.

28 (*a*) S. Fukuzumi, K. Ohkubo, Y. Tokuda and T. Suenobu, *J. Am. Chem. Soc.*, 2000, **122**, 4286; (*b*) R. S. Mulliken and W. B. Person, *Molecular Complexes. A Lecture and Reprint Volume*, Wiley-Interscience, New York, 1969; (*c*) R. Foster, *Organic Charge-Transfer Complexes*, Academic Press, New York, 1969.

29 K. G. Thomas, V. Biju, D. M. Guldi, P. V. Kamat and M. V. George, *J. Phys. Chem. B*, 1999, **103**, 8864.

30 The extinction coefficient of $C_{60}^{\cdot-}$ has been reported as 12 000 M^{-1} cm^{-1}. See: D. R. Lawson, D. L. Feldheim, C. A. Foss, P. K. Dorhout, C. M. Elliott, C. R. Martin and B. Parkinson, *J. Electrochem. Soc.*, 1992, **139**, L68.

31 The transient absorption band at the NIR region (1050 nm) is clearly assigned to the C_{60} cluster radical anion since such an NIR absorption band is diagnostic of C_{60} radical anion ($C_{60}^{\cdot-}$). The small difference in the λ_{max} value (1050 nm) in Fig. 7A from that of $C_{60}^{\cdot-}$ (1080 nm) results from the molecular aggregation of the cluster radical anion (see: ref. 30). The λ_{max} values of absorption spectra of $C_{60}^{\cdot-}$ vary slightly depending on the molecular assembly properties.

32 Judging from the large driving force of photoinduced electron transfer from I^- to the singlet excited state of C_{60} (1.3 eV), the photoinduced electron transfer may occur at the diffusion-limited rate. In such a case, the concentration of I^- (0.50 mol dm^{-3}) is large enough to quench the singlet excited state of C_{60} by the electron transfer reduction of I^-. The electron transfer from I^- to the triplet excited state of C_{60} is also exergonic ($\Delta G = -0.9$ V) and thus both the singlet and triplet excited states of C_{60} may be involved in the photoinduced electron transfer reduction of $I^{\cdot-}$. The excitation energies of the singlet and triplet excited states of C_{60} have been reported as 1.99 and 1.57 eV, respectively. See: R. M. Williams, J. M. Zwier and J. W. Verhoeven, *J. Am. Chem. Soc.*, 1995, **117**, 4093.

33 S. Fukuzumi, I. Nakanishi, T. Suenobu and K. M. Kadish, *J. Am. Chem. Soc.*, 1999, **121**, 3468.

34 The power conversion efficiency at high input power (100 mW cm^{-2}) decreases to 0.055%.